Hypersingular formulation for boundary strain evaluation in the context of a CTO-based implicit BEM scheme for small strain elasto-plasticity.

Marc Bonnet, H. Poon, S. Mukherjee

Hypersingular formulation for boundary strain evaluation in the context of a CTO-based implicit BEM scheme for small strain elasto-plasticity

Marc Bonnet
Laboratoire de Mécanique des Solides, CNRS URA 317
centre commun Polytechnique, Mines, Ponts et Chausées
Ecole Polytechnique, Palaiseau, France

Harrison Poon† and Subrata Mukherjee
Dept. of Theoretical and Applied Mechanics, Cornell University
Ithaca, NY 14853, USA

International Journal of Plasticity, **14**:1033–1058 (1998)

ABSTRACT

Boundary element method (BEM) formulations for usual and sensitivity problems in small strain elastoplasticity, using the concept of the consistent tangent operator (CTO), have been recently proposed by Bonnet, Mukherjee and Poon. "Usual" problems here refer to analysis of nonlinear problems in structural and solid continua, for which Simo and Taylor first proposed use of the CTO within the context of the finite element method (FEM). The BEM approach is shown to work well in the illustrative numerical examples in the papers by Bonnet, Mukherjee and Poon.

Stresses on the boundary of a body must be computed accurately in order for the CTO-based algorithm to work. There are at least two approaches for calculating boundary stresses in the BEM. The first involves local tangential differentiation of the shape functions of boundary displacements, together with the local use of constitutive equations. The second is the use of a hypersingular BEM formulation. The first approach has been used in the previous work mentioned above, while the second is employed in the present work.

† Currently: National Center for Supercomputing Applications, University of Illinois at Urbana - Champaign, Urbana, IL 61801, USA

Here, a new algorithm is proposed for regularization of hypersingular BEM equations for elastoplastic problems. Numerical results are presented for the elastoplastic equivalents of the Lame and Kirsch problems in two-dimensional linear elasticity. The results are compared with FEM and are seen to be acceptably accurate.

1. Introduction

Boundary element method (BEM) formulations for usual and sensitivity problems in small strain elasto-plasticity, using the concept of the consistent tangent operator (CTO), have been recently proposed by Bonnet and Mukherjee [1996] and Poon *et al.*[1996]. Usual problems here refer to analysis of nonlinear problems in structural and solid continua, for which Simo and Taylor [1985] first proposed use of the CTO within the context of the implicit finite element method (FEM). The CTO plays a pivotal role in this work. It enhances the mathematical elegance of the implicit approach by furnishing the exact derivative for the Newton-Rhapson procedure that is used to solve nonlinear algebraic equations that arise in the implicit formulation. Quadratic convergence of the Newton Rhapson method is achieved when the CTO is employed. Also, the CTO makes possible accurate computation of design sensitivities. The basic BEM formulation, together with a one-dimensional (1-D) numerical implementation, are presented in Bonnet and Mukherjee [1996], while a general numerical implementation for two-dimensional (2-D) plane strain problems appears in Poon *et al.*[1996]. The reader is referred to, for example, Vidal and Haber [1993], Kleiber *et al.*[1994] and Michaleris *et al.*[1994] for FEM based sensitivity analysis of nonlinear problems with the CTO.

Stresses on the boundary of a body must be computed accurately in order for the CTO based implicit algorithm to work properly. There are at least two approaches for calculating boundary stresses in the BEM. The first involves local tangential differentiation of the shape functions that are used to interpolate the boundary displacements, together with pointwise application of Hooke's law (e.g. Zhang *et al.*, [1992]). This method, referred to in the present paper as the "boundary shortcut", has been employed in Poon *et al.* [1996]. The second is the careful regularization of the hypersingular integral representations. This latter approach is adopted in the present paper.

Hypersingular integrals, and their role in the BEM, is a subject of considerable current research interest. A recent review article by Tanaka *et al.*[1994], for example, cites 350 references! An updated review of hypersingular integral equations can be found in Paulino [1995], while complex variable formulations for 2-D potential problems appear in Kolhe *et al.*[1996]. It is fair to say that most research papers to date, that are concerned with hypersingular integrals, address linear problems. On the other hand, the "boundary shortcut" approach is popular for BEM analyses of elasto-plastic problems. Examples of the latter are Poon *et al.*[1996], Telles and Carrer [1991], Sladek and Sladek [1995] and Sladek and Sladek [1995]. The paper by Leitao *et al.*[1995] does contain a hypersingular integral expression for the stress at a smooth boundary point for elasto-plastic problems. This expression, however, is not regularized, but contains Cauchy Principal Value (CPV) and Hadamard Finite Part (HFP) integrals. In the numerical implementation, the authors used semi-discontinuous interpolation for internal cells adjacent to the boundary, thereby forcing all collocation nodes to be internal.

In the present work, a hypersingular representation for boundary displacement gradients in elasto-plasticity is completely regularized using a novel approach. This idea transfers tangential derivatives from the singular kernels to the displacements so that the final regularized form contains, at most, weakly singular kernels. This approach uses traction and displacement data (the latter in the form of tangential derivatives) over the **entire** boundary, as opposed to strictly local information that is used in the "shortcut" method.

A just published paper by Huber *et al.*[1996] has come to the authors' attention upon completion of the writing of the present paper. In this paper, the authors have derived a 3-D hypersingular BIE for elastoplasticity and have used it to compute surface stresses. Their method is an extension of the approach proposed by Guiggiani *et al.*[1992] for linear elasticity. The present paper proposes a different regularization approach from theirs. Also, the present paper uses the CTO in an implicit BEM while Huber *et al.*[1996] do not use the CTO in their work.

Ideally, C^1 elements, for discretization of both the geometry and boundary variables, should be used in the present work. Here, however, standard isoparametric quadratic C^0 elements are used. Slope continuity of the domain boundary (across boundary elements) is

enforced using a special construction proposed by Guiggiani (private communication, detailed in part 1 of appendix A), while a continuous boundary interpolation of the displacement tangential gradient results from a "least squares fit" idea presented in Polch *et al.*[1987]. Numerical results are presented for the elasto-plastic counterparts of the Lamé and Kirsch problems in 2-D linear elasticity. Corners on the boundary are not modeled in this work. This is a subject for future research. It is important to mention again that the formulation presented in this paper is valid for general elasto-plastic problems, within the small strain assumption. Numerical results, presented for certain illustrative examples, are seen to be acceptably accurate. The smoothing approaches due to Guiggiani and Polch *et al.*[1987], mentioned above, are seen to be crucial for the success of the numerical scheme. It is expected that the use of C^1 elements would further improve the accuracy of the numerical solutions. This will be attempted in the future.

2. Implicit BEM solution scheme for elasto-plasticity

This section summarizes, for the sake of completeness, the CTO-based BEM solution strategy for small strain elasto-plasticity proposed in Bonnet and Mukherjee [1996] and Poon *et al.*[1996].

The boundary integral equation (BIE) (without body forces) in the presence of plastic strain reads:

$$\int_{\partial\Omega} [u_i(\boldsymbol{z}) - u_i(\boldsymbol{x})] P_i^k(\boldsymbol{x},\boldsymbol{z}) dS_z - \int_{\partial\Omega} p_i(\boldsymbol{z}) U_i^k(\boldsymbol{x},\boldsymbol{z}) dS_z = \int_{\Omega} U_{i,j}^k(\boldsymbol{x},\boldsymbol{z}) C_{ijab} \varepsilon_{ab}^p(\boldsymbol{z}) dV_z \qquad (1)$$

where $\boldsymbol{x}$ is any fixed source point on the boundary $\partial\Omega$, and $\boldsymbol{p}$, $\boldsymbol{u}$, ε^p denote the traction, displacement, and plastic strain, respectively. U_i^k, P_i^k are the Kelvin displacement and traction kernels. The variable field point is denoted by $\boldsymbol{z}$ and $_{,j} \equiv \partial/\partial \boldsymbol{z}_j$. The tensor C_{ijkl} is the usual Hookean elasticity tensor, which, for isotropic elasticity, has the form

$$C_{ijkl} = \frac{2G\nu}{1-2\nu}\delta_{ij}\delta_{kl} + G(\delta_{ik}\delta_{jl} + \delta_{il}\delta_{jk})$$

where G is the shear modulus, ν the Poisson's ratio and $\boldsymbol{\delta}$ is the Kronecker delta.

The matrix equation obtained by discretizing the above BIE reads:

$$[\boldsymbol{H}]\{\boldsymbol{u}\} - [\boldsymbol{G}]\{\boldsymbol{p}\} = [\boldsymbol{Q}]\{\boldsymbol{C} : \boldsymbol{\varepsilon}^p\}$$

which, after the standard operation of "collecting" boundary unknowns, becomes ($\boldsymbol{y}$ being the vector of boundary unknowns):

$$[\boldsymbol{A}]\{\boldsymbol{y}\} = \{\boldsymbol{f}\} + [\boldsymbol{Q}]\{\boldsymbol{C} : \boldsymbol{\varepsilon}^p\} \tag{2}$$

Next, the displacement at an internal point is given by:

$$\begin{aligned} u_k(\boldsymbol{x}) = &\int_{\partial\Omega} \left\{ p_i(\boldsymbol{z}) U_i^k(\boldsymbol{x},\boldsymbol{z}) - u_i(\boldsymbol{z}) P_i^k(\boldsymbol{x},\boldsymbol{z}) \right\} dS_z \\ &+ \int_{\Omega} U_{i,j}^k(\boldsymbol{x},\boldsymbol{z}) C_{ijab} \varepsilon_{ab}^p(\boldsymbol{z}) dV_z \end{aligned} \tag{3}$$

which, after differentiation w.r.t. x_ℓ and regularization, yields:

$$\begin{aligned} u_{k,\ell}(\boldsymbol{x}) = &\int_{\partial\Omega} u_i(\boldsymbol{z}) P_{i,\ell}^k(\boldsymbol{x},\boldsymbol{z}) dS_z - \int_{\partial\Omega} p_i(\boldsymbol{z}) U_{i,\ell}^k(\boldsymbol{x},\boldsymbol{z}) dS_z \\ &- C_{ijab} \varepsilon_{ij}^p(\boldsymbol{x}) \int_{\partial\Omega} n_\ell(\boldsymbol{z}) U_{a,b}^k(\boldsymbol{x},\boldsymbol{z}) dS_z \\ &- \int_{\Omega} U_{i,j\ell}^k(\boldsymbol{x},\boldsymbol{z}) C_{ijab} [\varepsilon_{ab}^p(\boldsymbol{z}) - \varepsilon_{ab}^p(\boldsymbol{x})] dV_z \end{aligned} \tag{4}$$

The well-known kinematic relationship between strain components and displacement gradients allows us to write:

$$\begin{aligned} \{\boldsymbol{\varepsilon}\} &= [\boldsymbol{G}']\{\boldsymbol{p}\} - [\boldsymbol{H}']\{\boldsymbol{u}\} + [\boldsymbol{Q}']\{\boldsymbol{C} : \boldsymbol{\varepsilon}^p\} \\ &= -[\boldsymbol{A}']\{\boldsymbol{y}\} + \{\boldsymbol{f}'\} + [\boldsymbol{Q}']\{\boldsymbol{C} : \boldsymbol{\varepsilon}^p\} \end{aligned} \tag{5}$$

Note that certain integrals in (4) become hypersingular when $\boldsymbol{x}$ lies on the boundary. In fact, a computable, fully regularized boundary strain representation is the central theme of this paper. This will be discussed in detail in the next section. For now, suffice to say that the strain at a boundary point is expressable in terms of boundary tractions and displacements and domain plastic strains, as given in (5) above.

Substituting for $\{\boldsymbol{y}\}$ from (2) into (5) yields:

$$\{\boldsymbol{\varepsilon}\} = \{\boldsymbol{n}\} + [\boldsymbol{S}]\{\boldsymbol{C} : \boldsymbol{\varepsilon}^p\} \tag{6}$$

where

$$\{\boldsymbol{n}\} = \{\boldsymbol{f}'\} - [\boldsymbol{A}'][\boldsymbol{A}]^{-1}\{\boldsymbol{f}\}$$

$$[\boldsymbol{S}] = [\boldsymbol{Q}'] - [\boldsymbol{A}'][\boldsymbol{A}]^{-1}[\boldsymbol{Q}]$$

Note that $\{\boldsymbol{n}\}$ denotes the purely elastic solution, i.e. the one obtained for the same loading but in the absence of plastic strain.

At this point we recall Hooke's law and the additive decomposition of strain:

$$\boldsymbol{\sigma} = \boldsymbol{C} : (\boldsymbol{\varepsilon} - \boldsymbol{\varepsilon}^p) \tag{7}$$

or

$$\{\boldsymbol{C} : \boldsymbol{\varepsilon}^p\} = \{\boldsymbol{C} : \boldsymbol{\varepsilon}\} - \{\boldsymbol{\sigma}\}$$

giving:

$$\{\boldsymbol{\varepsilon}\} = \{\boldsymbol{n}\} + [\boldsymbol{S}](\{\boldsymbol{C} : \boldsymbol{\varepsilon}\} - \{\boldsymbol{\sigma}\})$$

or

$$[\boldsymbol{S}]\{\boldsymbol{\sigma} - \boldsymbol{C}\boldsymbol{\varepsilon}\} - \{\boldsymbol{n}\} + [\boldsymbol{I}]\{\boldsymbol{\varepsilon}\} = \{\boldsymbol{0}\} \tag{8}$$

with the corresponding incremental form:

$$[\boldsymbol{S}]\{\Delta\boldsymbol{\sigma}_n - \boldsymbol{C}\Delta\boldsymbol{\varepsilon}_n\} - \{\Delta n_n\} + [\boldsymbol{I}]\{\Delta\boldsymbol{\varepsilon}_n\} = \{\boldsymbol{0}\} \tag{9}$$

This is as far as we can get using equilibrium principles (Somigliana's identity) and the elastic Hooke's law. To proceed further, we need a discretized form of the elasto-plastic constitutive relation, one that relates $\Delta\boldsymbol{\sigma}_n$ to $\Delta\boldsymbol{\varepsilon}_n$. This is accomplished by the Radial Return Algorithm (RRA) (Simo and Taylor [1985]). Conceptually, the RRA serves the following function:

Input:	$\boldsymbol{\sigma}_n$, $\boldsymbol{\varepsilon}_n$, $\bar{e}^p_n$, $\Delta\boldsymbol{\varepsilon}_n$
Output:	$\bar{\boldsymbol{\sigma}} = \boldsymbol{\sigma}_{n+1}$ and $\bar{e}^p_{n+1}$

The consistent tangent operator (CTO), denoted in the present paper by $\boldsymbol{C}_{n+1}$, comes from "differentiating" the RRA. Being a fourth order tensor, it provides a linear mapping from an infinitesimal perturbation in the input strain increment $\delta\Delta\boldsymbol{\varepsilon}_n$ to the corresponding infinitesimal change in the output stress $\delta\bar{\boldsymbol{\sigma}}$:

$$\boldsymbol{C}_{n+1} = \frac{\partial\bar{\boldsymbol{\sigma}}}{\partial\Delta\boldsymbol{\varepsilon}_n}$$

Both the RRA and the CTO are explained in detail in Simo and Taylor [1985] and briefly summarized in Bonnet and Mukherjee [1996].

Combining the equilibrium and constitutive equations in the form

$$\{\boldsymbol{\sigma}_n\} + \{\Delta\boldsymbol{\sigma}_n\} = \{\bar{\boldsymbol{\sigma}}\}$$

(where $\Delta\boldsymbol{\sigma}_n(\Delta\boldsymbol{\varepsilon}_n, \cdot\cdot, \cdot\cdot)$ comes from the BEM equation (9) while $\bar{\boldsymbol{\sigma}}(\Delta\boldsymbol{\varepsilon}_n, \cdot\cdot, \cdot\cdot)$ (which is $\boldsymbol{\sigma}_{n+1}$) comes from the RRA), we obtain a nonlinear equation for $\Delta\boldsymbol{\varepsilon}_n$ of the form:

$$\{G(\Delta\boldsymbol{\varepsilon}_n)\} \equiv [\boldsymbol{S}]\{\bar{\boldsymbol{\sigma}}(\boldsymbol{\varepsilon}_n, \boldsymbol{\sigma}_n, \bar{e}^p_n, \Delta\boldsymbol{\varepsilon}_n) - \boldsymbol{\sigma}_n - \boldsymbol{C}\Delta\boldsymbol{\varepsilon}_n\} - \{\Delta n_n\} + [\boldsymbol{I}]\{\Delta\boldsymbol{\varepsilon}_n\} = \{\boldsymbol{0}\} \quad (10)$$

The consistent tangent operator $\boldsymbol{C}_{n+1}$ appears upon application of Newton's method. The additive correction $\delta\boldsymbol{\varepsilon}^i_n = \Delta\boldsymbol{\varepsilon}^{i+1}_n - \Delta\boldsymbol{\varepsilon}^i_n$ to $\Delta\boldsymbol{\varepsilon}^i_n$ solves the equation

$$([\boldsymbol{S}][\boldsymbol{C} - \boldsymbol{C}^i_{n+1}] - [\boldsymbol{I}])\{\delta\boldsymbol{\varepsilon}^i_n\} = \{G(\Delta\boldsymbol{\varepsilon}^i_n)\} \quad (11)$$

The quantity $([\boldsymbol{S}][\boldsymbol{C} - \boldsymbol{C}^i_{n+1}] - [\boldsymbol{I}]) = ([\boldsymbol{D}^i_{n+1}] - [\boldsymbol{I}])$ is hereafter called the global CTO (see Kleiber *et al.*[1994] for the FEM version). Once the nonlinear equation (10) is solved for $\Delta\boldsymbol{\varepsilon}_n$, all the variables at time t_{n+1} are readily computed. It is interesting to note that the Newton step (11) involves the difference $[\boldsymbol{C} - \boldsymbol{C}^i_{n+1}]$ between the elastic constitutive law and the local CTO, rather than the local CTO itself; this is entirely consistent with the fact that eqn (9) accounts for equilibrium as well as the elastic constitutive law. Because of the difference $[\boldsymbol{C} - \boldsymbol{C}^i_{n+1}]$, a matrix partitioning scheme exists whereby the effective system size depends only on the size of the plastically deforming zone. This is explained in Poon *et al.*[1996].

It is worth mentioning that the current CTO-based formulation lends itself to accurate sensitivity computations. An accompanying sensitivity formulation (not shown in this paper) reveals that the stiffness matrix for the (linear) sensitivity problem is precisely the converged value of the global CTO. The reader is referred to Poon *et al.*[1996] for details.

3. Hypersingular boundary strain computation

The primary motivation behind the present paper is the observation that, when the "boundary shortcut" (local tangential differentiation of the shape functions interpolating the boundary displacements, together with pointwise application of Hooke's law) is used in conjunction with eqn (5), the numerical results can exhibit fluctuations around the reference solution. This is reported for the elastic case in Guiggiani [1994] and for the elastoplastic case in Poon *et al.*[1996]. The use of shape function differentiation, and the localized nature of the shortcut, are believed to contribute to the error. Attempts to avoid the shortcut, by dealing carefully with the hypersingular boundary strain (or stress) representation, can lead to more accurate results. This is demonstrated for the elastic case in Guiggiani [1994]. Elastoplastic problems are considered in the present work. It is found, however, that for the numerical examples considered in this paper, both the "shortcut" and hypersingular numerical results compare well with finite element method (FEM) results.

A computable formula for the integral representation of the displacement gradient $u_{a,b}(\boldsymbol{x})$ (and hence the strain) at a boundary point $\boldsymbol{x}$ in the presence of initial (e.g. plastic) strain $\boldsymbol{\varepsilon}^p$ is developed, within the context of small strain elastoplasticity. The formula is derived using an indirect regularization technique, and applies with fair generality in 2D or 3D situations. The numerical examples, however, are restricted to the specific case of 2D plane strain deformation.

It is a convenient practice that, when collocating at a boundary point, we introduce an exclusion (or inclusion) zone and deform the boundary accordingly (Figure 1). The size of the exclusion zone, as well as the distortion of the boundary, tend to zero by a limiting process. By explicitly integrating over $(\partial\Omega - e_\epsilon) + s_\epsilon$, this approach avoids special interpretations of boundary integrals (e.g. in the Cauchy principal value sense) and the companion specification of "corner" tensors. The choice between exclusion and inclusion neighborhoods is rather immaterial. The representation formulae differ only by the source point displacement. As indicated in Figure 1, we opt for the exclusion zone.

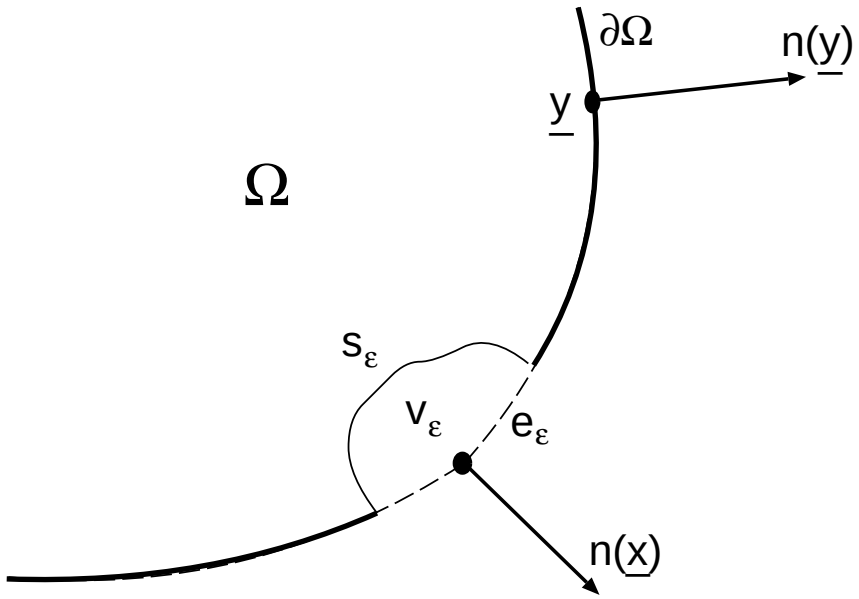

Figure 1. Source point and exclusion neighborhood

3.1 Indirect regularization approach

The starting point is the exterior representation formula for the domain Ω_ϵ with boundary $(\partial\Omega - e_\epsilon) + s_\epsilon$, which reads

$$0 = \int_{(\partial\Omega - e_\epsilon)+s_\epsilon} \left\{ P_i^k(\boldsymbol{x},\boldsymbol{y}) u_i(\boldsymbol{y}) - U_i^k(\boldsymbol{x},\boldsymbol{y}) p_i(\boldsymbol{y}) \right\} dS_y \\ - \int_{\Omega_\epsilon} \Sigma_{ij}^k(\boldsymbol{x},\boldsymbol{y}) \varepsilon_{ij}^p(\boldsymbol{y}) dV_y \tag{12}$$

where Σ_{ij}^k is the Kelvin stress kernel. A regularization of (12) will be followed by the limiting process $\varepsilon \to 0$.

The first step involves regularization of the domain integral. Consider the purely plastic state

$$v_i(\boldsymbol{y}) = \varepsilon_{ij}^p(\boldsymbol{x}) y_j \qquad \boldsymbol{\sigma}(\boldsymbol{y}) = \mathbf{0}\,,\ \boldsymbol{p}(\boldsymbol{y}) = \mathbf{0} \tag{13}$$

(note that the constant strain tensor $\varepsilon_{ij}^p(\boldsymbol{x})$ is geometrically compatible). The exterior representation formula for the above plastic state reads

$$0 = \varepsilon_{ij}^p(\boldsymbol{x}) \left\{ \int_{(\partial\Omega - e_\epsilon)+s_\epsilon} P_i^k(\boldsymbol{x},\boldsymbol{y}) y_j(\boldsymbol{y}) dS_y - \int_{\Omega_\epsilon} \Sigma_{ij}^k(\boldsymbol{x},\boldsymbol{y}) dV_y \right\} \tag{14}$$

Subtracting (14) from (12), one gets:

$$
\begin{aligned}
0 = & \int_{(\partial\Omega - e_\epsilon)+s_\epsilon} \left\{ P_i^k(\boldsymbol{x},\boldsymbol{y}) u_i(\boldsymbol{y}) - U_i^k(\boldsymbol{x},\boldsymbol{y}) p_i(\boldsymbol{y}) \right\} dS_y \\
& - \varepsilon_{ij}^p(\boldsymbol{x}) \int_{(\partial\Omega - e_\epsilon)+s_\epsilon} P_i^k(\boldsymbol{x},\boldsymbol{y}) y_j(\boldsymbol{y}) dS_y \\
& - \int_{\Omega_\epsilon} \Sigma_{ij}^k(\boldsymbol{x},\boldsymbol{y}) \left[\varepsilon_{ij}^p(\boldsymbol{y}) - \varepsilon_{ij}^p(\boldsymbol{x}) \right] dV_y
\end{aligned} \tag{15}
$$

Next, the derivative of Eq. (15) with respect to x_ℓ is taken, resulting in

$$
\begin{aligned}
0 = & \int_{(\partial\Omega - e_\epsilon)+s_\epsilon} \left\{ P_{i,\bar{\ell}}^k(\boldsymbol{x},\boldsymbol{y}) u_i(\boldsymbol{y}) - U_{i,\bar{\ell}}^k(\boldsymbol{x},\boldsymbol{y}) p_i(\boldsymbol{y}) \right\} dS_y \\
& - \varepsilon_{ij}^p(\boldsymbol{x}) \int_{(\partial\Omega - e_\epsilon)+s_\epsilon} P_{i,\bar{\ell}}^k(\boldsymbol{x},\boldsymbol{y}) y_j(\boldsymbol{y}) dS_y \\
& - \int_{\Omega_\epsilon} \Sigma_{ij,\bar{\ell}}^k(\boldsymbol{x},\boldsymbol{y}) \left[\varepsilon_{ij}^p(\boldsymbol{y}) - \varepsilon_{ij}^p(\boldsymbol{x}) \right] dV_y \\
& - \varepsilon_{ij,\bar{\ell}}^p(\boldsymbol{x}) \left\{ \int_{(\partial\Omega - e_\epsilon)+s_\epsilon} P_i^k(\boldsymbol{x},\boldsymbol{y}) y_j(\boldsymbol{y}) dS_y - \int_{\Omega_\epsilon} \Sigma_{ij}^k(\boldsymbol{x},\boldsymbol{y}) dV_y \right\}
\end{aligned} \tag{16}
$$

Since $\varepsilon_{ij}^p(\boldsymbol{x})$ in the identity (14) is arbitrary, one readily notes that the expression multiplying $\varepsilon_{ij,\bar{\ell}}^p(\boldsymbol{x})$ (i.e. the last line) in the above formula vanishes. Notations like $U_{i,\ell}^k$ and $U_{i,\bar{\ell}}^k$, respectively, denote derivatives of kernel functions with respect to y_ℓ and x_ℓ. Furthermore, the Kelvin solution has the property that $U_{i,\bar{\ell}}^k = -U_{i,\ell}^k$.

One important hallmark of the present regularization approach is the transfer of derivatives from the kernel to the field variable, by means of integration by parts. The order of singularity of the kernel is reduced at the expense of having to deal with (tangential) derivatives of field variables.

The differential operator:

$$
f \to D_{ab} f = n_a f_{,b} - n_b f_{,a}
$$

where n_a is the unit outward normal, has the property that

$$
\int_S D_{ab} f \, \mathrm{d}S = 0 \tag{17}
$$

for any piecewise regular closed surface S and any continuous and piecewise differentiable function f. Using this identity, one can effect the following transformation, for a generic boundary field variable $f(\boldsymbol{y})$

$$\begin{aligned}
&\int_{(\partial\Omega-e_\epsilon)+s_\epsilon} P^k_{i,\bar{\ell}}(\boldsymbol{x},\boldsymbol{y}) f(\boldsymbol{y}) dS_y \\
&= -\int_{(\partial\Omega-e_\epsilon)+s_\epsilon} \Sigma^k_{ij,\ell}(\boldsymbol{x},\boldsymbol{y}) n_j(\boldsymbol{y}) f(\boldsymbol{y}) dS_y \\
&= -\int_{(\partial\Omega-e_\epsilon)+s_\epsilon} \left\{ D_{j\ell}\Sigma^k_{ij}(\boldsymbol{x},\boldsymbol{y}) + \underbrace{\Sigma^k_{ij,j}(\boldsymbol{x},\boldsymbol{y})}_{=0} n_\ell(\boldsymbol{y}) \right\} f(\boldsymbol{y}) dS_y \\
&= \int_{(\partial\Omega-e_\epsilon)+s_\epsilon} \Sigma^k_{ij}(\boldsymbol{x},\boldsymbol{y}) D_{j\ell} f dS_y
\end{aligned} \tag{18}$$

In the foregoing derivation, use has been made of the fact that $\Sigma^k_{ij,j} = 0$ for any $\boldsymbol{y} \neq \boldsymbol{x}$, together with the following "antisymmetric" property of the operator D_{ab}:

$$\int_S g D_{ab} f \, \mathrm{d}S = -\int_S f D_{ab} g \, \mathrm{d}S$$

the proof of which involves a trivial application of the product rule.

The major accomplishment of formula (18) is to reduce the kernel from hypersingular to strongly singular, meanwhile shifting a tangential derivative to the field variable f.

Application of formula (18) to (16) (with $f = u_i$ and $f = y_j$) gives

$$\begin{aligned}
0 = &\int_{(\partial\Omega-e_\epsilon)+s_\epsilon} \left\{ \Sigma^k_{ij}(\boldsymbol{x},\boldsymbol{y}) D_{j\ell} u_i(\boldsymbol{y}) + U^k_{i,\ell}(\boldsymbol{x},\boldsymbol{y}) p_i(\boldsymbol{y}) \right\} dS_y \\
&- \varepsilon^p_{i\ell}(\boldsymbol{x}) \underbrace{\int_{(\partial\Omega-e_\epsilon)+s_\epsilon} P^k_i(\boldsymbol{x},\boldsymbol{y}) dS_y}_{=0} + \varepsilon^p_{ij}(\boldsymbol{x}) \int_{(\partial\Omega-e_\epsilon)+s_\epsilon} \Sigma^k_{ij}(\boldsymbol{x},\boldsymbol{y}) n_\ell(\boldsymbol{y}) dS_y \\
&- \int_{\Omega_\epsilon} \Sigma^k_{ij,\bar{\ell}}(\boldsymbol{x},\boldsymbol{y}) \left[\varepsilon^p_{ij}(\boldsymbol{y}) - \varepsilon^p_{ij}(\boldsymbol{x}) \right] dV_y
\end{aligned} \tag{19}$$

The domain integral, being weakly singular, can be handled by a mapping method (see, e.g. Lean and Wexler [1985]) . Our immediate goal is to regularize the boundary integrals. To this end, we appeal to additive strain decomposition and Hooke's law:

$$\boldsymbol{C} : \boldsymbol{\varepsilon}^p = \boldsymbol{C} : \boldsymbol{\varepsilon} - \boldsymbol{\sigma}$$

or

$$\boldsymbol{\varepsilon}^p = \boldsymbol{\varepsilon} - \boldsymbol{C}^{-1} : \boldsymbol{\sigma}$$

The collection of boundary integrands in (19) is transformed as follows:

$$\begin{aligned}
&\Sigma_{ij}^k(\boldsymbol{x},\boldsymbol{y})D_{j\ell}u_i(\boldsymbol{y}) - U_{i,\bar{\ell}}^k(\boldsymbol{x},\boldsymbol{y})p_i(\boldsymbol{y}) + \Sigma_{ij}^k(\boldsymbol{x},\boldsymbol{y})n_\ell(\boldsymbol{y})\varepsilon_{ij}^p(\boldsymbol{x}) \\
=&\Sigma_{ij}^k(\boldsymbol{x},\boldsymbol{y})n_j(\boldsymbol{y})u_{i,\ell}(\boldsymbol{y}) + \Sigma_{ij}^k(\boldsymbol{x},\boldsymbol{y})n_\ell(\boldsymbol{y})[u_{i,j}(\boldsymbol{x}) - u_{i,j}(\boldsymbol{y})] \\
&- U_{i,j}^k(\boldsymbol{x},\boldsymbol{y})n_\ell(\boldsymbol{y})\sigma_{ij}(\boldsymbol{x}) - U_{i,\bar{\ell}}^k(\boldsymbol{x},\boldsymbol{y})n_j(\boldsymbol{y})\sigma_{ij}(\boldsymbol{y}) \\
=&P_i^k(\boldsymbol{x},\boldsymbol{y})u_{i,\ell}(\boldsymbol{y}) + \Sigma_{ij}^k(\boldsymbol{x},\boldsymbol{y})n_\ell(\boldsymbol{y})[u_{i,j}(\boldsymbol{x}) - u_{i,j}(\boldsymbol{y})] \\
&+ U_{i,\ell}^k(\boldsymbol{x},\boldsymbol{y})n_j(\boldsymbol{y})[\sigma_{ij}(\boldsymbol{y}) - \sigma_{ij}(\boldsymbol{x})] + D_{j\ell}U_i^k(\boldsymbol{x},\boldsymbol{y})\sigma_{ij}(\boldsymbol{x})
\end{aligned}$$

Eq. (19) therefore becomes

$$\begin{aligned}
0 = &\int_{(\partial\Omega - e_\epsilon)+s_\epsilon} P_i^k(\boldsymbol{x},\boldsymbol{y})[u_{i,\ell}(\boldsymbol{y}) - u_{i,\ell}(\boldsymbol{x})]dS_y \\
&+ \int_{(\partial\Omega - e_\epsilon)+s_\epsilon} \Sigma_{ij}^k(\boldsymbol{x},\boldsymbol{y})n_\ell(\boldsymbol{y})[u_{i,j}(\boldsymbol{x}) - u_{i,j}(\boldsymbol{y})]dS_y \\
&+ \int_{(\partial\Omega - e_\epsilon)+s_\epsilon} U_{i,\ell}^k(\boldsymbol{x},\boldsymbol{y})n_j(\boldsymbol{y})[\sigma_{ij}(\boldsymbol{y}) - \sigma_{ij}(\boldsymbol{x})]dS_y \\
&- \int_{\Omega_\epsilon} \Sigma_{ij,\bar{\ell}}^k(\boldsymbol{x},\boldsymbol{y})\left[\varepsilon_{ij}^p(\boldsymbol{y}) - \varepsilon_{ij}^p(\boldsymbol{x})\right] dV_y
\end{aligned} \tag{20}$$

Identity (17) for $f = U_i^k(\boldsymbol{x},\boldsymbol{y})$ on the closed surface $(\partial\Omega - e_\epsilon) + s_\epsilon$ has been used, together with the following one which holds true because $\boldsymbol{x}$ is exterior to the closed surface $(\partial\Omega - e_\epsilon) + s_\epsilon$:

$$u_{i,\ell}(\boldsymbol{x}) \int_{(\partial\Omega - e_\epsilon)+s_\epsilon} P_i^k(\boldsymbol{x},\boldsymbol{y})dS_y = 0$$

At this point, if we make the further assumption that $\nabla\boldsymbol{u} \in C^{0,\alpha}$ at $\boldsymbol{x}$, then all integrals over s_ε in (20) vanish in the limit $\varepsilon \to 0$, while all integrals over $\partial\Omega - e_\varepsilon$ are convergent in the ordinary sense. The regularization is complete.

The validity of the assumption $\nabla\boldsymbol{u} \in C^{0,\alpha}$ warrants careful investigation. Two immediate difficulties are spelled out as follows:

(i) It is shown in Timoshenko and Goodier [1970] that $\nabla\boldsymbol{u}$ is not continuous at general corners, even for linear elasticity.

(ii) At a smooth boundary point, the continuity of both $\nabla \boldsymbol{u}$ and the unit tangent implies a continuous tangential derivative $\partial \boldsymbol{u}/\partial s$. However, this physical continuity is violated in the discretization process at the end nodes of C^0 elements if one computes the tangential derivative by shape function differentiation.

As far as the above difficulties are concerned:

(i) The present numerical examples do not contain sharp corners and it is assumed that $\nabla \boldsymbol{u} \in C^{0,\alpha}$.

(ii) The proper way to handle it is by using C^1 elements, such as Overhauser and Hermite. Here we apply the idea in Polch *et al.*[1987] who developed the idea in the context of 3D crack problems. Simply put, a new C^0 interpolation for du/ds is introduced, in such a way that it approximates the shape function differentiation of (the C^0 interpolation of) u in a least squares sense. This tactic is henceforth referred to as the "smoothing technique" and is explained in Appendix A.

Getting back to the hypersingular formulation, we note that the limiting form of eq. (20) is not suitable for our application, because the complete displacement gradient at a field point $u_{i,j}(\boldsymbol{y})$ is not available from the boundary displacement interpolation. Further transformation of (20) is needed.

3.2 Reformulation of the strain representation formula

In view of the corner difficulty mentioned earlier, from now on, we deal strictly with smooth points on the boundary.

Consider a partition $\partial\Omega = E_1 + \ldots + E_M + \Gamma$ of $\partial\Omega$, where $E_1, \ldots, E_M$ are the M elements sharing $\boldsymbol{x}$ (Figure 2).

We are seeking a practically computable form for the limit when $\varepsilon \to 0$ in eq. (20), that is:

$$
\begin{aligned}
0 = &\int_{\partial\Omega - e_\varepsilon} P_i^k(\boldsymbol{x},\boldsymbol{y})[u_{i,\ell}(\boldsymbol{y}) - u_{i,\ell}(\boldsymbol{x})]dS_y \\
&+ \int_{\partial\Omega - e_\varepsilon} \Sigma_{ij}^k(\boldsymbol{x},\boldsymbol{y}) n_\ell(\boldsymbol{y})[u_{i,j}(\boldsymbol{x}) - u_{i,j}(\boldsymbol{y})]dS_y \\
&+ \int_{\partial\Omega - e_\varepsilon} U_{i,\ell}^k(\boldsymbol{x},\boldsymbol{y}) n_j(\boldsymbol{y})[\sigma_{ij}(\boldsymbol{y}) - \sigma_{ij}(\boldsymbol{x})]dS_y
\end{aligned}
$$

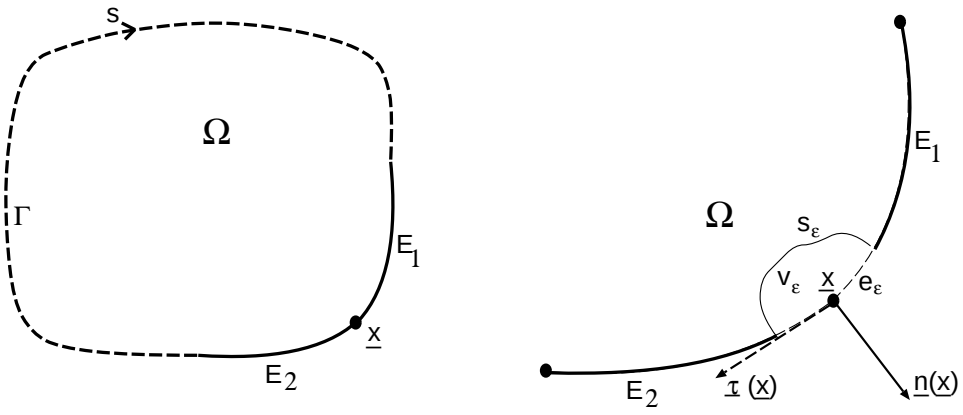

Figure 2. Boundary partitioning

$$-\int_\Omega \Sigma^k_{ij,\bar{\ell}}(\boldsymbol{x},\boldsymbol{y})\left[\varepsilon^p_{ij}(\boldsymbol{y})-\varepsilon^p_{ij}(\boldsymbol{x})\right]dV_y+O(\varepsilon)$$

accounting for the fact that integrals over s_ε vanish in the limit and the domain integral is convergent.

First, the integrands containing the unwanted field point displacement gradients are transformed as follows:

$$\begin{aligned}
&P^k_i(\boldsymbol{x},\boldsymbol{y})u_{i,\ell}(\boldsymbol{y})-\Sigma^k_{ij}(\boldsymbol{x},\boldsymbol{y})n_\ell(\boldsymbol{y})u_{i,j}(\boldsymbol{y})\\
&=\Sigma^k_{ij}(\boldsymbol{x},\boldsymbol{y})n_j(\boldsymbol{y})u_{i,\ell}(\boldsymbol{y})-\Sigma^k_{ij}(\boldsymbol{x},\boldsymbol{y})n_\ell(\boldsymbol{y})u_{i,j}(\boldsymbol{y})\\
&=\Sigma^k_{ij}(\boldsymbol{x},\boldsymbol{y})D_{j\ell}u_i(\boldsymbol{y})
\end{aligned}\tag{21}$$

Then, the boundary is split according to the partition $\partial\Omega-e_\varepsilon=(E_1-e_\varepsilon)+\ldots+(E_M-e_\varepsilon)+\Gamma$ defined above. Using (21) at the singular point $\boldsymbol{x}$ for the integrals over E_m-e_ε, we get (with appropriate addition-subtractions and some cancellations)

$$\begin{aligned}
0=&\int_\Gamma \Sigma^k_{ij}(\boldsymbol{x},\boldsymbol{y})D_{j\ell}u_i(\boldsymbol{y})dS_y+\int_\Gamma U^k_{i,\ell}(\boldsymbol{x},\boldsymbol{y})p_i(\boldsymbol{y})dS_y\\
&+\sum_{m=1}^{M}\left\{\int_{E_m-e_\varepsilon}\Sigma^k_{ij}(\boldsymbol{x},\boldsymbol{y})[D^m_{j\ell}u_i(\boldsymbol{y})-D^m_{j\ell}u_i(\boldsymbol{x})]dS_y\right.\\
&\left.+\int_{E_m-e_\varepsilon}U^k_{i,\ell}(\boldsymbol{x},\boldsymbol{y})[p_i(\boldsymbol{y})-p_i(\boldsymbol{x})]dS_y\right\}\\
&-\int_\Omega \Sigma^k_{ij,\bar{\ell}}(\boldsymbol{x},\boldsymbol{y})\left[\varepsilon^p_{ij}(\boldsymbol{y})-\varepsilon^p_{ij}(\boldsymbol{x})\right]dV_y+C_{k\ell}(\boldsymbol{x},\varepsilon)+O(\varepsilon)
\end{aligned}\tag{22}$$

with

$$
\begin{aligned}
C_{k\ell}(\boldsymbol{x},\varepsilon) = &- u_{i,\ell}(\boldsymbol{x}) \int_\Gamma P_i^k(\boldsymbol{x},\boldsymbol{y}) dS_y + u_{i,j}(\boldsymbol{x}) \int_\Gamma \Sigma_{ij}^k(\boldsymbol{x},\boldsymbol{y}) n_\ell(\boldsymbol{y}) dS_y \\
&- u_{i,\ell}(\boldsymbol{x}) \sum_{m=1}^{M} \int_{E_m - e_\varepsilon} \Sigma_{ij}^k(\boldsymbol{x},\boldsymbol{y}) [n_j^m(\boldsymbol{y}) - n_j^m(\boldsymbol{x})] dS_y \\
&+ u_{i,j}(\boldsymbol{x}) \sum_{m=1}^{M} \int_{E_m - e_\varepsilon} \Sigma_{ij}^k(\boldsymbol{x},\boldsymbol{y}) [n_\ell^m(\boldsymbol{y}) - n_\ell^m(\boldsymbol{x})] dS_y \\
&- \sigma_{ij}(\boldsymbol{x}) \int_\Gamma U_{i,\ell}^k(\boldsymbol{x},\boldsymbol{y}) n_j(\boldsymbol{y}) dS_y \\
&- \sigma_{ij}(\boldsymbol{x}) \sum_{m=1}^{M} \int_{E_m - e_\varepsilon} U_{i,\ell}^k(\boldsymbol{x},\boldsymbol{y}) [n_j^m(\boldsymbol{y}) - n_j^m(\boldsymbol{x})] dS_y
\end{aligned} \tag{23}
$$

Finally, since all integrals over $E_m - e_\varepsilon$ that appear in (22) and (23) are regular, the limiting form for $\varepsilon \to 0$ exists, and its expression follows at once:

$$
\begin{aligned}
0 = &\int_\Gamma \Sigma_{ij}^k(\boldsymbol{x},\boldsymbol{y}) D_{j\ell} u_i(\boldsymbol{y}) dS_y + \int_\Gamma U_{i,\ell}^k(\boldsymbol{x},\boldsymbol{y}) p_i(\boldsymbol{y}) dS_y \\
&+ \sum_{m=1}^{M} \left\{ \int_{E_m} \Sigma_{ij}^k(\boldsymbol{x},\boldsymbol{y}) [D_{j\ell}^m u_i(\boldsymbol{y}) - D_{j\ell}^m u_i(\boldsymbol{x})] dS_y \right. \\
&\left. + \int_{E_m} U_{i,\ell}^k(\boldsymbol{x},\boldsymbol{y}) [p_i(\boldsymbol{y}) - p_i(\boldsymbol{x})] dS_y \right\} \\
&+ \int_\Omega C_{ijab} U_{a,b\ell}^k(\boldsymbol{x},\boldsymbol{y}) \left[\varepsilon_{ij}^p(\boldsymbol{y}) - \varepsilon_{ij}^p(\boldsymbol{x}) \right] dV_y + C_{k\ell}(\boldsymbol{x})
\end{aligned} \tag{24}
$$

with

$$
\begin{aligned}
C_{k\ell}(\boldsymbol{x}) = &- u_{i,\ell}(\boldsymbol{x}) \int_\Gamma P_i^k(\boldsymbol{x},\boldsymbol{y}) dS_y + u_{i,j}(\boldsymbol{x}) \int_\Gamma \Sigma_{ij}^k(\boldsymbol{x},\boldsymbol{y}) n_\ell(\boldsymbol{y}) dS_y \\
&- u_{i,\ell}(\boldsymbol{x}) \sum_{m=1}^{M} \int_{E_m} \Sigma_{ij}^k(\boldsymbol{x},\boldsymbol{y}) [n_j^m(\boldsymbol{y}) - n_j^m(\boldsymbol{x})] dS_y \\
&+ u_{i,j}(\boldsymbol{x}) \sum_{m=1}^{M} \int_{E_m} \Sigma_{ij}^k(\boldsymbol{x},\boldsymbol{y}) [n_\ell^m(\boldsymbol{y}) - n_\ell^m(\boldsymbol{x})] dS_y \\
&- \sigma_{ij}(\boldsymbol{x}) \int_\Gamma U_{i,\ell}^k(\boldsymbol{x},\boldsymbol{y}) n_j(\boldsymbol{y}) dS_y \\
&- \sigma_{ij}(\boldsymbol{x}) \sum_{m=1}^{M} \int_{E_m} U_{i,\ell}^k(\boldsymbol{x},\boldsymbol{y}) [n_j^m(\boldsymbol{y}) - n_j^m(\boldsymbol{x})] dS_y
\end{aligned} \tag{25}
$$

Note that the domain integral has been transformed into a form more suitable for our symbolic strain representation, eq. (5).

3.3 Transition to 2D plane strain

Notice that eq. (13), when applied to 2D plane strain, precludes the existence of ε^p_{33}. This is physically incorrect and the formulae developed in the previous sub-section should be regarded as 3D results. Fortunately, the corresponding plane strain formulae assume identical forms. This can be seen by treating plane strain as a special 3D configuration:

$$\Omega = D\times]-\infty,+\infty[\qquad \partial\Omega = \partial D\times]-\infty,+\infty[$$
$$\boldsymbol{u}(\boldsymbol{y}) = u_1(y_1,y_2)\boldsymbol{e}_1 + u_2(y_1,y_2)\boldsymbol{e}_2$$
$$\boldsymbol{p}(\boldsymbol{y}) = t_1(y_1,y_2)\boldsymbol{e}_1 + t_2(y_1,y_2)\boldsymbol{e}_2$$

Then, the integrals are re-interpreted in a manner such as the following:

$$\int_{\partial\Omega} U^k_{i,\ell}(\boldsymbol{x},\boldsymbol{y})p_i(\boldsymbol{y})dS_y = \int_{\partial D} \underbrace{\int_{-\infty}^{-\infty} U^k_{i,\ell}(\boldsymbol{x},\boldsymbol{y})dy_3}_{U^k_{i,\ell} \text{ in plane strain}} \; p_i(y_1,y_2)ds_y$$

Moreover, it turns out that the following is true for the Kelvin solution

$$\int_{-\infty}^{+\infty} U^k_{3,3\ell}(\boldsymbol{x},\boldsymbol{y})dy_3 = 0$$

so that the terms containing ε^p_{33} in eq. (24) vanish in the y_3-integration process. Formulae (24) and (25) are then formally identical in 2D plane strain and 3D, provided the appropriate kernels are used.

Also, the operator $D_{ab}f$ has an additional interpretation in 2D:

$$f \to D_{ab}f = n_a f_{,b} - n_b f_{,a} = e_{ba} f_{,\tau}$$

where e_{ba} is the 2D alternating tensor, and $_{,\tau}$ denotes the partial derivative along the unit tangent (tangential derivative). Note: the orientation of the unit tangent $\boldsymbol{t}$ is such that $\boldsymbol{t}\times\boldsymbol{n} = \boldsymbol{e}_3$.

Referring back to formulae (24) and (25), one notices the coupling among the displacement gradient components (bear in mind that k and ℓ are the free indices). The pertinent components being sought (for the purpose of getting strain components) are $u_{1,1}$, $u_{2,2}$, $u_{1,2}$

and $u_{2,1}$. By ranging the free indices k, ℓ from 1 to 2, one can form a system of 4 equations involving the 4 sought-after unknowns. The 4 by 4 system can then be easily inverted, either numerically through Gaussian elimination, or "exactly" through Cramer's rule, to recover the individual $u_{1,1}$, $u_{2,2}$, $u_{1,2}$ and $u_{2,1}$. These are then easily translated into strain components ε_{ij}. The other side of the equation will contain, besides the nodal tractions and plastic strains, displacement tangential derivatives over the boundary. These in turn, are related to the boundary nodal displacements through the "smoothing technique". The end result is that the symbolic strain representation from the previous section (eq. (5))

$$\{\boldsymbol{\varepsilon}\} = [\boldsymbol{G}']\{\boldsymbol{p}\} - [\boldsymbol{H}']\{\boldsymbol{u}\} + [\boldsymbol{Q}']\{\boldsymbol{C} : \boldsymbol{\varepsilon}^p\}$$

is preserved.

3.4 Domain partitioning into a potentially plastic part and its complement

For computational efficiency, the domain discretization should be done only for the potentially plastic zone. The 2D domain Ω is partitioned into Ω_P, which is potentially plastic and covered with internal cells, and its complement Ω_C, which remains elastic and not discretized. The objective of this section is to transform the domain integral in eq. (24) into one which integrates over Ω_P only, with appropriate modifications of certain boundary integrals. We introduce some new notations as shown in Figure 3, and note that, for $\boldsymbol{x} \in \Gamma_P$:

$$\begin{aligned}
&\int_\Omega C_{ijab} U^k_{a,b\ell}(\boldsymbol{x},\boldsymbol{y}) \left[\varepsilon^p_{ij}(\boldsymbol{y}) - \varepsilon^p_{ij}(\boldsymbol{x})\right] dV_y \\
&= \int_{\Omega_P} C_{ijab} U^k_{a,b\ell}(\boldsymbol{x},\boldsymbol{y}) \left[\varepsilon^p_{ij}(\boldsymbol{y}) - \varepsilon^p_{ij}(\boldsymbol{x})\right] dV_y - \varepsilon^p_{ij}(\boldsymbol{x}) \int_{\Omega_C} \Sigma^k_{ij,\ell}(\boldsymbol{x},\boldsymbol{y}) dV_y \\
&= \int_{\Omega_P} C_{ijab} U^k_{a,b\ell}(\boldsymbol{x},\boldsymbol{y}) \left[\varepsilon^p_{ij}(\boldsymbol{y}) - \varepsilon^p_{ij}(\boldsymbol{x})\right] dV_y - \varepsilon^p_{ij}(\boldsymbol{x}) \int_{\Gamma_C \cup \Gamma_{PC}} \Sigma^k_{ij}(\boldsymbol{x},\boldsymbol{y}) n^C_\ell(\boldsymbol{y}) dS_y
\end{aligned}$$

where the superscript in n^C_ℓ specifies that the normal points away from Ω_C

$$\begin{aligned}
&= \int_{\Omega_P} C_{ijab} U^k_{a,b\ell}(\boldsymbol{x},\boldsymbol{y}) \left[\varepsilon^p_{ij}(\boldsymbol{y}) - \varepsilon^p_{ij}(\boldsymbol{x})\right] dV_y + \sigma_{ij}(\boldsymbol{x}) \int_{\Gamma_C \cup \Gamma_{PC}} U^k_{i,j}(\boldsymbol{x},\boldsymbol{y}) n^C_\ell(\boldsymbol{y}) dS_y \\
&\quad - \varepsilon_{ij}(\boldsymbol{x}) \int_{\Gamma_C \cup \Gamma_{PC}} \Sigma^k_{ij}(\boldsymbol{x},\boldsymbol{y}) n^C_\ell(\boldsymbol{y}) dS_y
\end{aligned}$$

where Hooke's law in the form of eq. (7) has been used

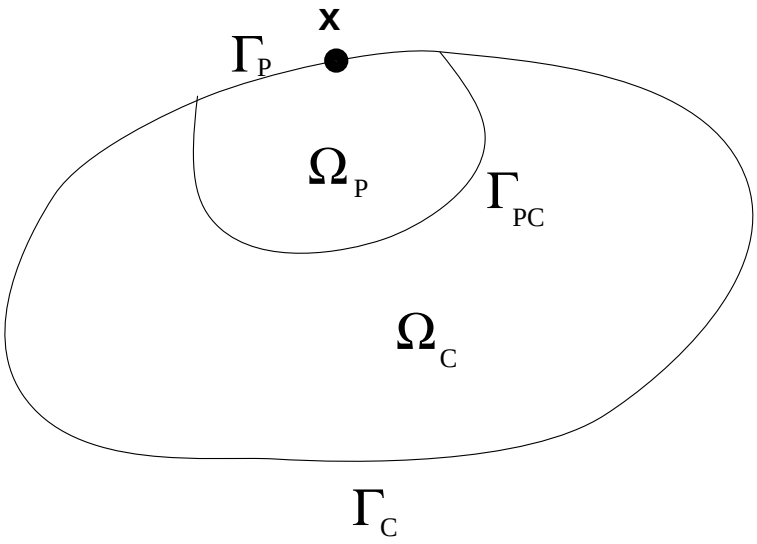

Figure 3. Domain partitioning

$$= \int_{\Omega_P} C_{ijab} U^k_{a,b\ell}(\boldsymbol{x},\boldsymbol{y}) \left[\varepsilon^p_{ij}(\boldsymbol{y}) - \varepsilon^p_{ij}(\boldsymbol{x})\right] dV_y + \sigma_{ij}(\boldsymbol{x}) \int_{\Gamma_C \cup \Gamma_{PC}} U^k_{i,\ell}(\boldsymbol{x},\boldsymbol{y}) n^C_j(\boldsymbol{y}) dS_y$$
$$- u_{i,j}(\boldsymbol{x}) \int_{\Gamma_C \cup \Gamma_{PC}} \Sigma^k_{ij}(\boldsymbol{x},\boldsymbol{y}) n^C_\ell(\boldsymbol{y}) dS_y$$

where identity (17) has been applied with $f = U^k_i$

In addition, $\int_{\Gamma_C \cup \Gamma_{PC}} P^k_i(\boldsymbol{x},\boldsymbol{y}) dS_y = 0$ since $\boldsymbol{x}$ lies outside Ω_C. It follows that, in expression (25) of $C_{k\ell}(\boldsymbol{x})$, the surface $\Gamma = \partial\Omega - \sum E_m$ must be replaced by $\tilde{\Gamma} = \Gamma_P \cup \Gamma_{PC} - \sum E_m$, i.e. by the nonsingular part of the boundary of the potentially plastic zone Ω_P. For $\boldsymbol{x} \in \Gamma_C$, the integration is still over $\Gamma = \partial\Omega - \sum E_m$. Of course, as mentioned before, the domain integral in eq. (24) is now over Ω_P.

A similar investigation has been carried out for the displacement gradient expression (4) at an internal point. The end result is that, for the practically useful case $\boldsymbol{x} \in \Omega_P$ (since only the plastic region Ω_P is meshed), the right hand side of eq. (4) must be modified as follows: replace $\partial\Omega$ in the third term by $\partial\Omega_P$ and Ω in the last term by Ω_P.

4. Numerical results

Two physical problems are solved, namely, a hollow cylinder subjected to internal pressure loading, and the stretching of a square plate with a circular hole. Both deform under plane strain conditions.

For both problems, the geometry and deformation modes are highly symmetric. For example, only one quarter needs to be modelled in the second example. However, the corners introduced by such exploitation of symmetry have not been addressed by the current treatise. As a consequence, both the cylinder and the square plate are modeled in full, with a complete circle as the inner boundary. Each of the outer corners of the square plate is approximated by a circular arc† with a finite, but negligible, radius of curvature.

Emphasis is on comparing the hypersingular approach to the "boundary shortcut". In the absence of closed form solutions, reference results are furnished by running the commercial finite element code ABAQUS [1995] on a fine mesh.

The hollow cylinder has inner radius 1 and outer radius 2. The square plate has inner radius 1 and outer side length 4. The elastic constants are: $G = 1, \quad \nu = 0.3$ where G denotes the shear modulus and ν the Poisson ratio. The material deforms plastically according to the classical J2 theory, with isotropic strain hardening of the form:

$$\kappa = 2G(0.001 + 0.001(\bar{e}^p)^m)$$

where (Poon et al. [1996]), $\bar{e}^p$ is the equivalent plastic strain, defined as:

$$\bar{e}^p = \int_0^t \sqrt{\frac{2}{3}} \|\boldsymbol{d}^p(\tau)\| d\tau$$

in terms of the plastic strain rate $\boldsymbol{d}^p = \dot{\boldsymbol{\varepsilon}}^p$, and

$$\|\boldsymbol{d}^p(\tau)\| = +\sqrt{d_{ij} d_{ij}}$$

Further, the yield condition is:

$$f(\boldsymbol{s}, \kappa) = \|\boldsymbol{s}\| - \sqrt{\frac{2}{3}} \kappa(\bar{e}^p) = 0$$

where $\boldsymbol{s} = \boldsymbol{\sigma} - \frac{1}{3}(\mathrm{tr}\boldsymbol{\sigma})\boldsymbol{I}$ is the deviatoric stress and κ is the (isotropic) strain hardening function. Finally $m = 0.2$ (nonlinear strain hardening). The usual practice of non-dimensionalization (e.g. dividing stresses by the shear modulus, radial distances by the

† Actually, a distortion of such, constructed by the special means described in part 1 of Appendix A

inner radius, etc.) becomes unnecessary with the current choice of material and geometrical parameters.

Quadratic interpolation of nodal quantities is used in the present work. The BEM implementation uses 3-noded boundary elements and 6-noded, triangular internal cells. Only the potentially plastic zone Ω_P (see Figure 3) is discretized in all the elastoplastic examples. The FEM setup (ABAQUS) employs 8-noded quadrilateral elements.

In the legend boxes, "HBEM" and "SBEM" stand for hypersingular BEM and shortcut BEM respectively.

4.1 Example 1

The first example demonstrates the supreme accuracy of the present approach in the linearly elastic case. The hollow cylinder is subjected to a small internal pressure of 10^{-4}, which is below the pressure at first yield (recall the shear modulus is 1 and the initial Mises yield stress is 0.002.) The inner and outer boundaries of the hollow cylinder are each divided into 36 equal divisions. Stresses are also computed at some internal points. Excellent agreement is obtained at between the HBEM and Lamé's exact solution. Numerical results for the radial and hoop stresses, as functions of position along a radius of the cylinder, available in Poon (PhD thesis, Cornell University, USA).

4.2 Example 2

This example uses the mesh shown in Figure 4. The internal pressure is large enough so that the plastic front is roughly at $r = 1.5$. The internal cells are sufficient to cover the plastic zone. The entire load is applied in one single step, thanks to the power of the CTO. Figure 5shows the distribution of radial stress through the cylinder, computed from the HBEM and SBEM together with a fine mesh ABAQUS solution. The same is true in Figure 6for the distribution of hoop stress. The numerical results are acceptable, though

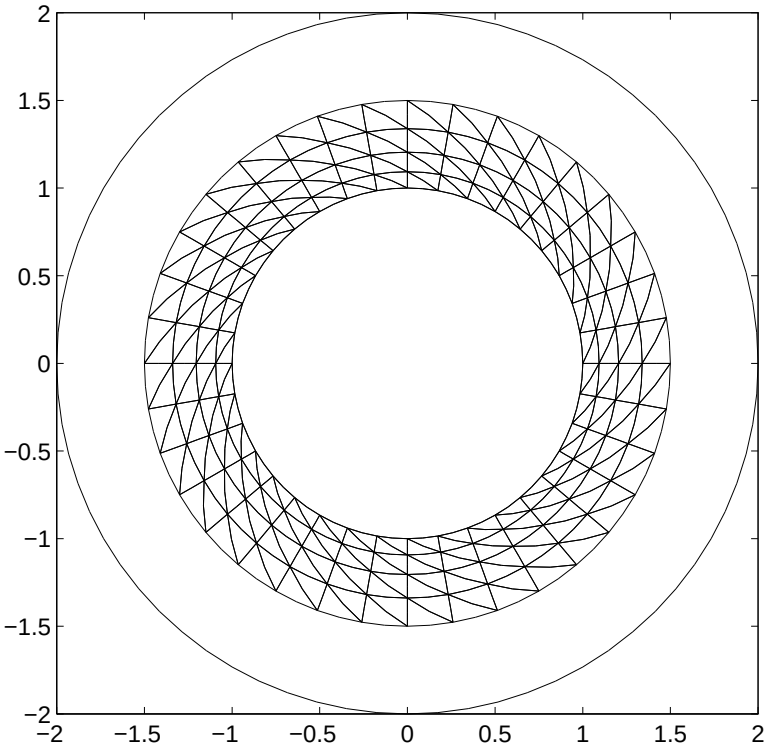

Figure 4. Example 2: BEM mesh

certainly not as accurate as in the linearly elastic case. The BEM results are those on the $\theta = 0$ radial segment – there are slight fluctuations in the θ direction, of the order of 1%.

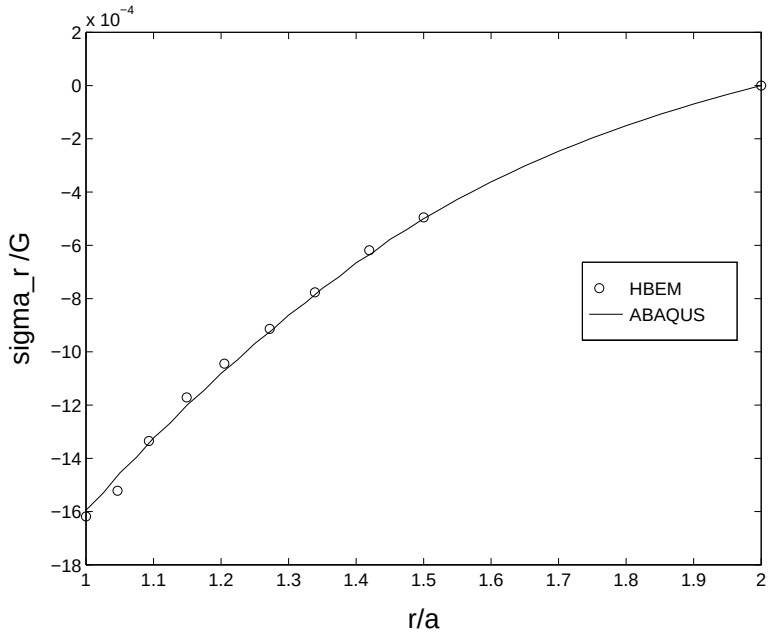

Figure 5. Example 2 (hypersingular and shortcut): radial stress

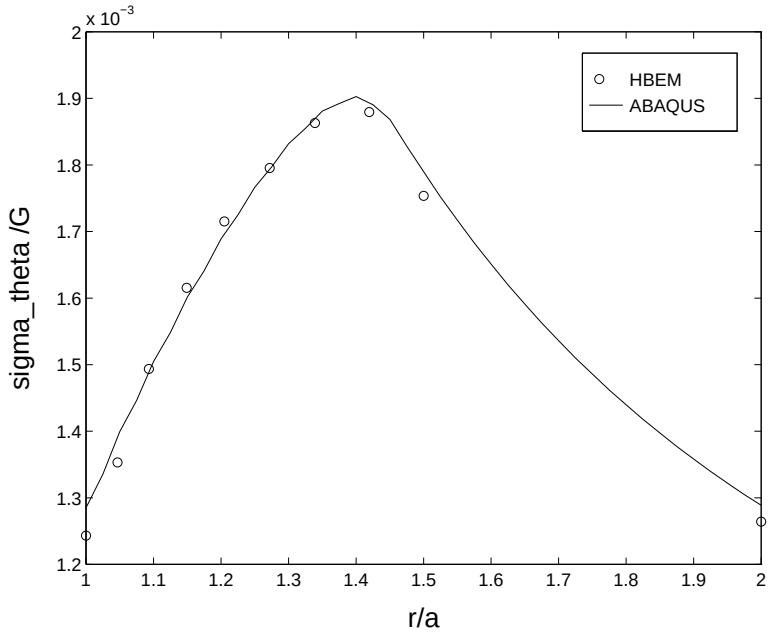

Figure 6. Example 2 (hypersingular and shortcut): hoop stress

Similar observations and comments apply in this example as in the previous one. The results from the "shortcut" and hypersingular approaches, in this case, are comparable.

4.3 Example 3

This example concerns the uniaxial stretching of a square plate with a circular hole. The geometry, loading, and axes convention are shown in Figure 7. For the sake of conciseness, each result is shown as a set of four sub-figures, arranged in the following manner:

- top left: σ_y at $y = 0$ as a function of x
- top right: Mises equivalent stress at $y = 0$ as a function of x
- bottom left: σ_θ at $r = 1$ as a function of θ
- bottom right: BEM mesh

The five results presented are:

◇ coarse mesh, linearly elastic, hypersingular: Figure 8

◇ coarse mesh, elastoplastic, hypersingular: Figure 9

◇ coarse mesh, elastoplastic, shortcut: Figure 10

◇ fine mesh, elastoplastic, hypersingular: Figure 11

◇ fine mesh, elastoplastic, shortcut: Figure 12

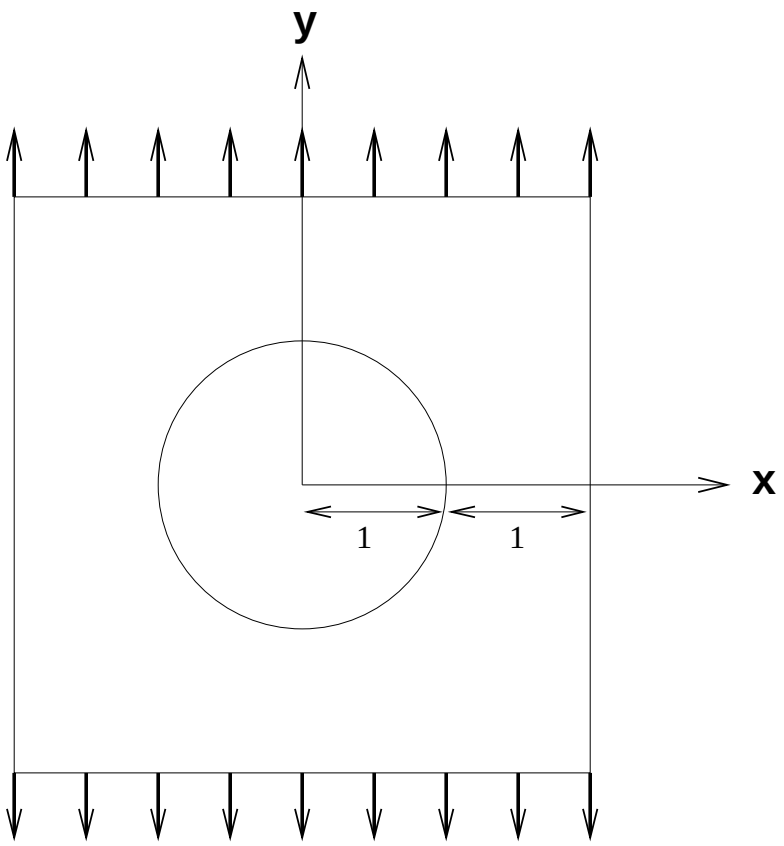

Figure 7. Example 3: Geometry, loading, and axes convention

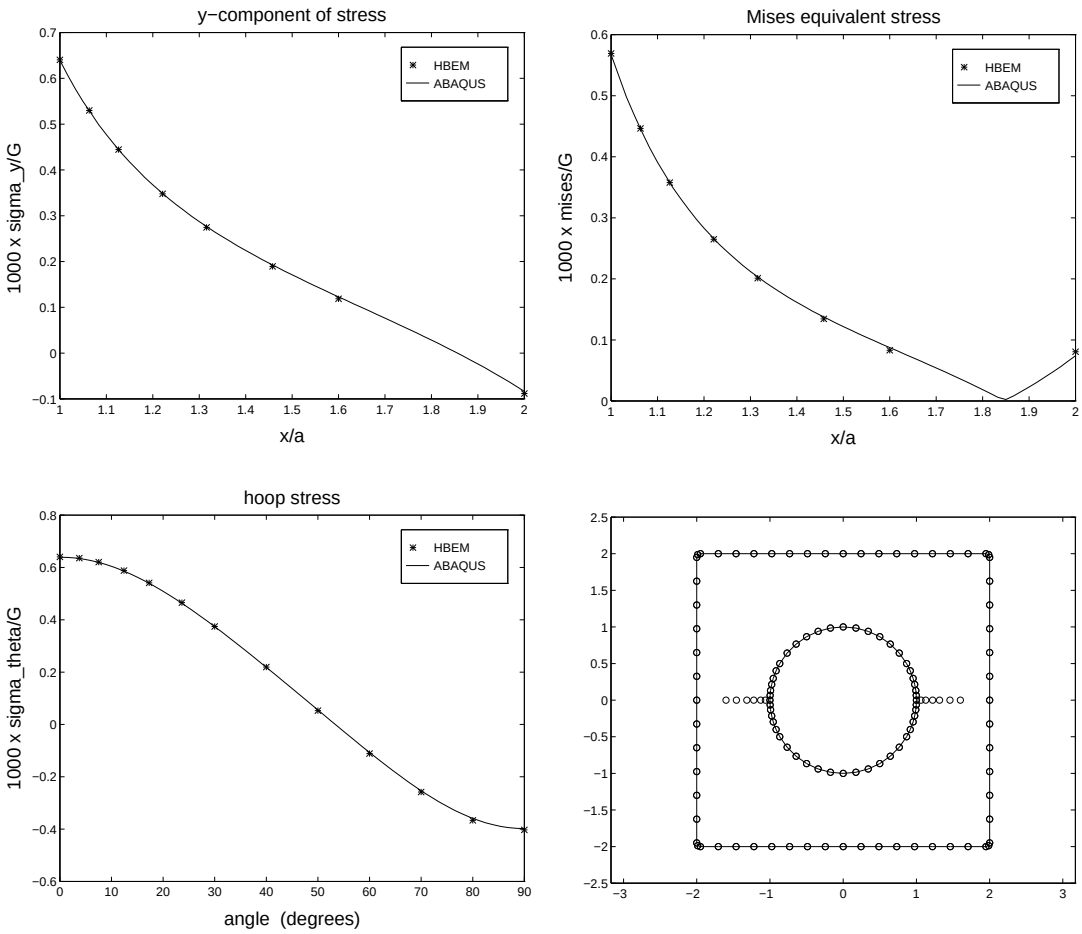

Figure 8. Example 3: coarse mesh, linearly elastic, hypersingular

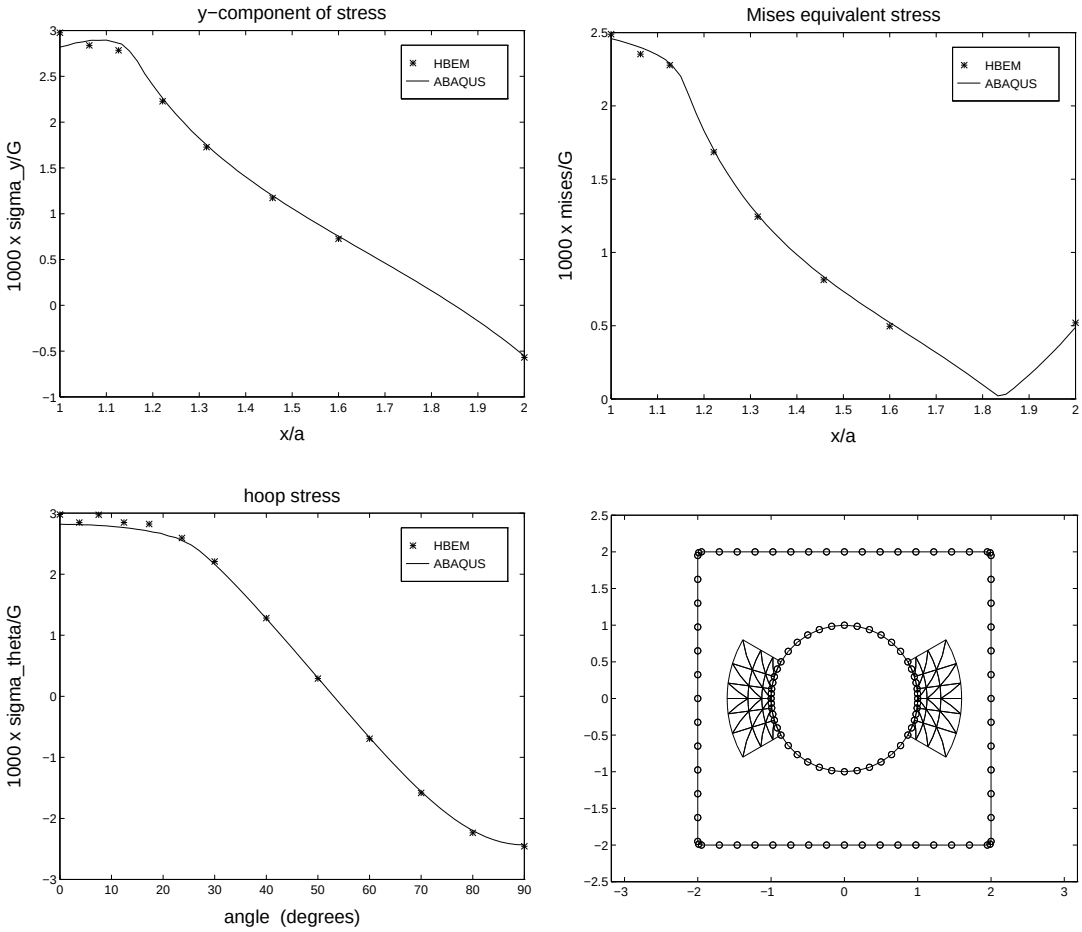

Figure 9. Example 3: coarse mesh, elastoplastic, hypersingular

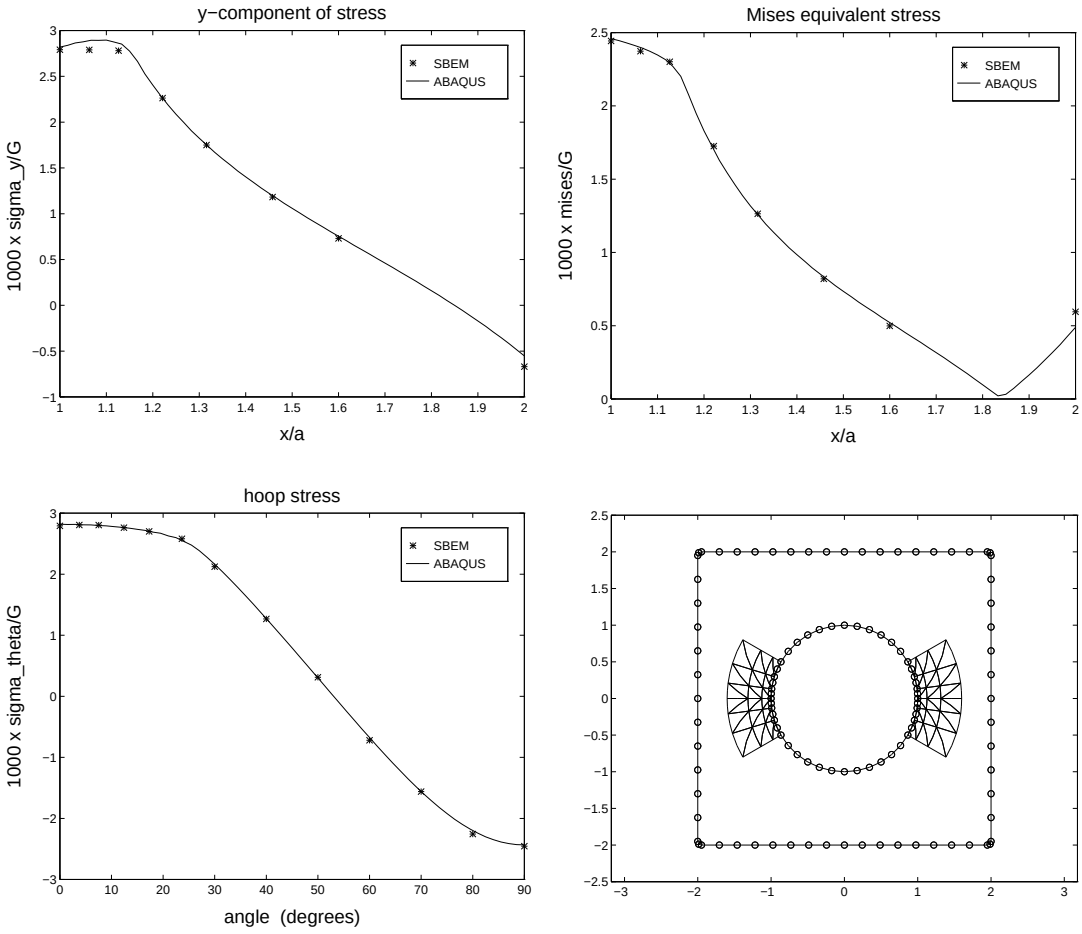

Figure 10. Example 3: coarse mesh, elastoplastic, shortcut

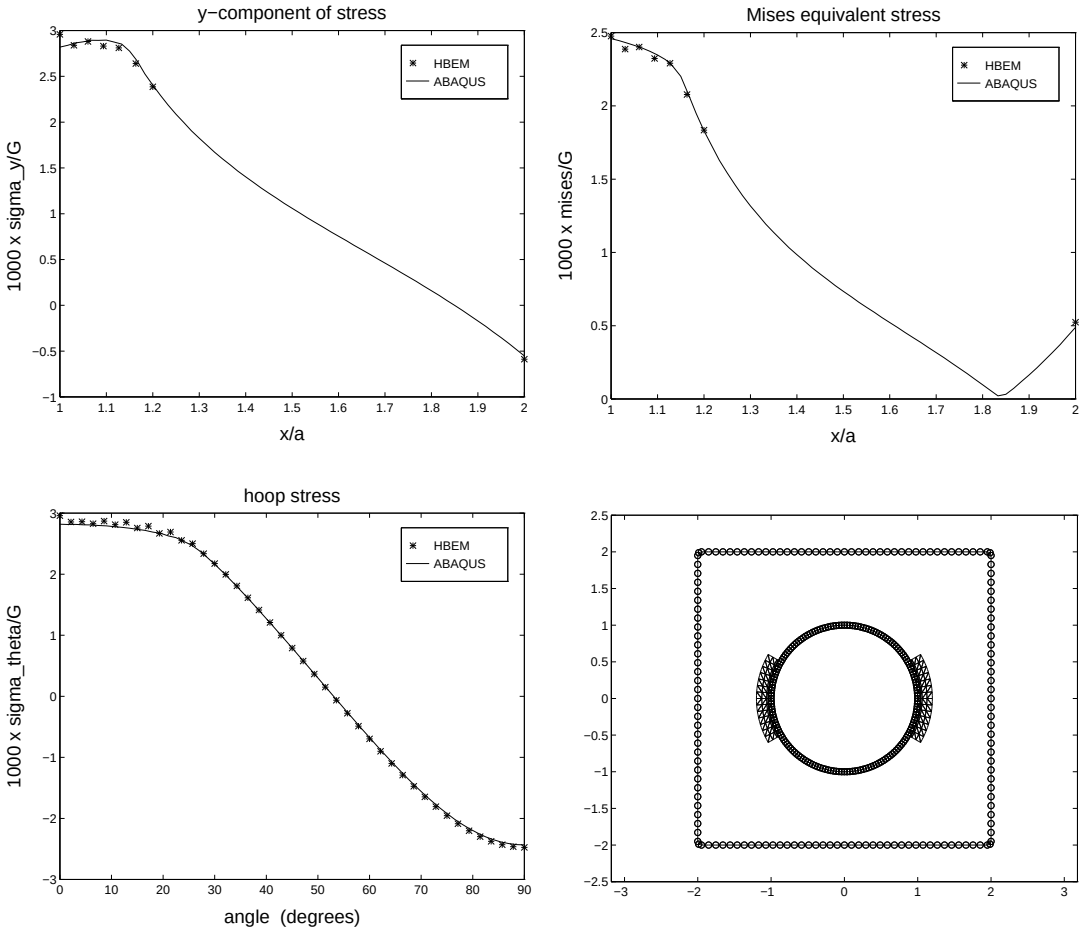

Figure 11. Example 3: fine mesh, elastoplastic, hypersingular

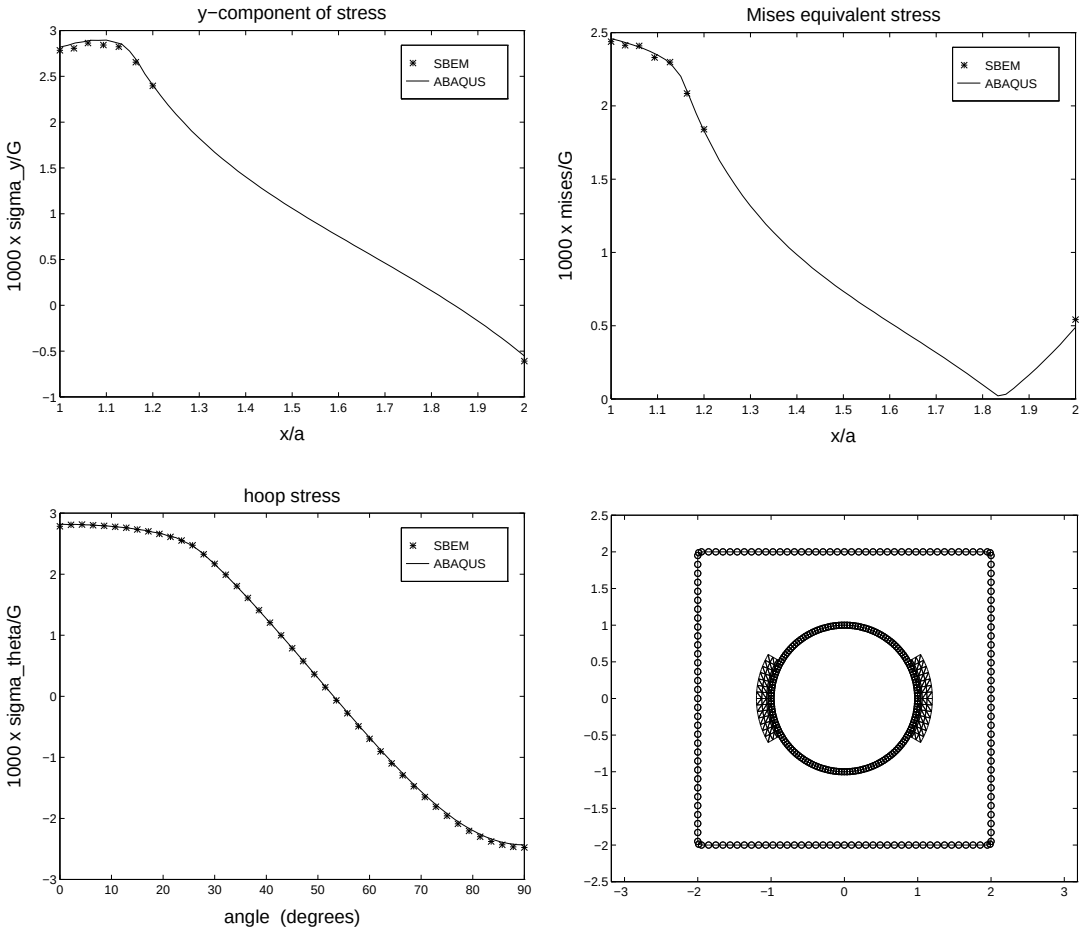

Figure 12. Example 3: fine mesh, elastoplastic, shortcut

Note the following pertinent remarks:

- ⋆ Apart from the linearly elastic case, all others share the same loading magnitude.
- ⋆ All cases are analyzed using one load step.
- ⋆ The circles in the BEM mesh denote nodes of the (quadratic) boundary elements. Unlike the hollow cylinder case, the boundary discretization cannot be inferred from the internal cells.
- ⋆ In the fine mesh cases, the area occupied by the internal cells barely covers the plastic zone.
- ⋆ The numerical results from both the "shortcut" and hypersingular approaches, especially with the fine mesh, are seen to agree well with the FEM results.

5. Conclusion

In conclusion, the present hypersingular algorithm represents a novel approach to deal with hypersingular kernels arising in the context of small strain elastoplasticity. The linearly elasic results turn out to be perfect. The elastoplastic results, while acceptably accurate, are expected to improve further with the adoption of C^1 boundary elements. Another possibility is the Galerkin BEM, where the continuity requirements are reduced and C^0 elements are sufficient.

Acknowledgements

This research was funded by NSF grant number MSS-9301443 to Cornell University. The computing for this research was conducted using the resources of the Cornell Theory Center, which receives major funding from the National Science Foundation and New York State with additional support from the Advanced Research Projects Agency, the National Center for Research Resources at the National Institutes of Health, IBM Corporation and members of the Corporate Research Institute.

REFERENCES

1970 Timoshenko S.P. and Goodier J.N., "Theory of Elasticity," McGraw-Hill,New York.

1985 Lean M.H. and Wexler A., "Accurate numerical integration of singular boundary element kernels over boundaries with curvature," Int. J. Num. Meth. in Eng., **21**, 211–228.

1985 Simo J.C. and Taylor R.L., "Consistent tangent operators for rate-independent elastoplasticity," Comp. Meth. in Appl. Mech. & Engng., **48**, 101–118.

1987 Polch E.Z., Cruse T.A., Huang C.J., "Traction BIE solutions for flat cracks," Comp. Mech., **2**, 253–267.

1991 Telles J.C.F. and Carrer J.A.M., "Implicit procedures for the solution of elastoplastic problems by the boundary element method," Mathl. Comput. Modelling., **15**, 303–311.

1992 Guiggiani M., Krishnasamy K., Rudolphi T. J. and Rizzo F. J., "A general algorithm for the numerical solution of hypersingular boundary integral equartions," J. Appl. Mech., **59**, 604-614.

1992 Zhang Q., Mukherjee S., and Chandra A., "Design sensitivity coefficients for elastoviscoplastic problems by boundary element methods," Int. J. Num. Meth. in Eng., **34**, 947–966.

1993 Vidal C.A. and Haber R.B., "Design sensitivity analysis for rate-independent elastoplasticity," Comp. Meth. in Appl. Mech. & Engng., **107**, 393–431.

1994 Guiggiani M., "Hypersingular formulation for boundary stress evaluation," Engng. Anal. with Bound. Elem., **13**, 169–179.

1994 Kleiber M., Hien T.D., and Postek E., "Incremental finite-element sensitivity analysis for non-linear mechanics applications," Int. J. Num. Meth. in Eng., **37**, 3291–3308.

1994 Michaleris P., Tortorelli D.A., and Vidal C.A., "Tangent operators and design sensitivity formulations for transient non-linear coupled problems with applications to elastoplasticity," Int. J. Num. Meth. in Eng., **37**, 2471–2499.

1994 Tanaka M., Sladek V. and Sladek J., "Regularization techniques applied to boundary element methods," Appl. Mech. Reviews, **47**, 457–499.

1995 ABAQUS Theory Manual, version 5.4, "," Hibbit, Karlsson and Sorensen, Inc.

1995 Leitao V., Aliabadi M. H., and Rooke D. P., "The dual boundary element formulation for elastoplastic fracture mechanics," Int. J. Num. Meth. in Eng., **38**, 315-333.

1995 Paulino G. H., "Novel formulations of the boundary element method for fracture mechanics and error estimation," Ph.D. dissertation, Cornell University, Ithaca, NY.

1995 Sladek J. and Sladek V., "Boundary Element for Thermoelastoplastic Problems," Int. J. Num. Meth. in Eng., **38**, 3635–3652.

1995 Sladek J. and Sladek V., "Boundary element analysis for an interface crack between dissimilar elastoplastic materials," Computational Mechanics, **16**, 396–405.

1996 Bonnet M. and Mukherjee S., "Implicit BEM formulations for usual and sensitivity problems in elasto-plasticity using the consistent tangent operator concept," Int. J. Solids Struct., **33**, 4461–4480.

1996 Huber O., Dallner R., Partheymuller P. and Kuhn G., "Evaluation of the stress tensor in 3-D elastoplasticity by direct solving of hypersingular integrals," Int. J. Num. Meth. in Eng., **39**, 2555–2573.

1996 Kolhe R., Ye W., Hui C.Y. and Mukherjee S., "Complex variable formulations for usual and hypersingular integral equations for potential problems – with applications to corners and cracks," Comp. Mech., **17**, 279–286.

1996 Poon H., Mukherjee S., and Bonnet M., "Numerical implementation of a CTO-based implicit approach for the BEM solution of usual and sensitivity problems in elasto-plasticity," Comp. & Struct., , accepted for publication.

Appendix A: smoothing technique

To illustrate the basic ideas, it suffices to consider two adjacent boundary elements:

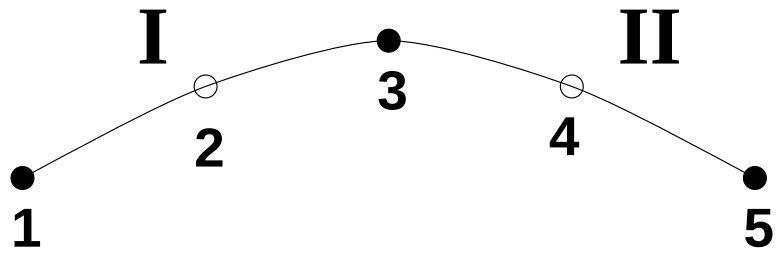

and the hypersingular boundary integral equation is being collocated at node 3.

(1) **Choice of mid-nodes** 2,4: the geometrical construction sketched below ensures a C^1 curve at node 3 (tangents at nodes 1,3,5 are prescribed by the user, location of nodes 2,4 is then deterministic):

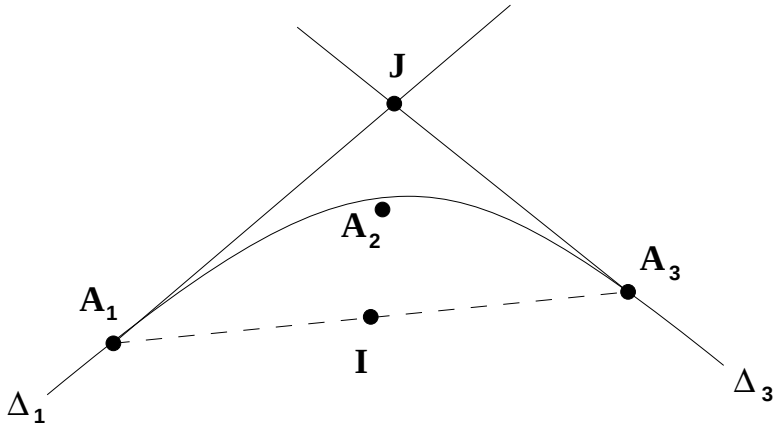

A_2 is the mid-point of $[I, J]$ with

$$J = \Delta_1 \cap \Delta_3$$

$$I = \text{midpoint of } [A_1, A_3]$$

Hermite interpolation is **not necessary** for C^1 curve generation. Note that

(i) Nodes A_1, A_3, tangents Δ_1, Δ_3 are "exact" (i.e. those of the exact curve being modelled).

(ii) Node A_2 is in general **not** located on the exact curve.

(2) **Tangential gradient interpolation**

¿From the usual C^0 interpolation:

$$\frac{du}{ds} = \frac{1}{J(\xi)} \sum_{k=1}^{5} \frac{dN_k}{d\xi} u_k$$

$s = s(\xi)$ on either E_I or E_{II}.

Idea: introduce a continuous interpolation

$$\frac{du}{ds} = \sum_{k=1}^{5} N_k(\xi) \left(\frac{du}{ds}\right)_k = \sum_{k=1}^{5} N_k(\xi) d_k$$

in terms of a new set of nodal values $d_k \equiv (du/ds)_k$

To relate the $\{d_k\}$ to the $\{u_k\}$, the following least-squares prolem is introduced:

$$\min_{\{d_k\}} \frac{1}{2} \int_{E_I \cup E_{II}} \left(\sum_{k=1}^{5} N_k d_k - \frac{1}{J} \sum_{k=1}^{5} \frac{dN_k}{d\xi} u_k \right)^2 \underbrace{J\, d\xi}_{ds}$$

i.e. the "new" interpolation must be closest (in the L^2 sense) to the "old" one.

The condition $\frac{\partial}{\partial d_\ell}(\frac{1}{2}\int \ldots d\xi) = 0$ for $1 \le \ell \le 5$ gives the set of linear equations:

$$\sum_{k=1}^{5} A_{\ell k} d_k = \sum_{k=1}^{5} B_{\ell k} u_k$$

where

$$A_{\ell k} = \int_{E_I \cup E_{II}} N_k N_\ell J\, d\xi$$

$$B_{\ell k} = \int_{E_I \cup E_{II}} \frac{dN_k}{d\xi} N_\ell\, d\xi$$

$[A]$ and $[B]$ are 5×5 matrices. Given the $\{u_k\}$ set, one solves for the $\{d_k\}$ set. Then the "new" interpolation is plugged in the singular integrals containing $\left(\frac{du}{ds}(y) - \frac{du}{ds}(x)\right)$ or similar quantities.

The extension of this basic idea to an arbitrary number of contiguous boundary elements is straightforward.

The idea for this C^0 interpolation for tangential gradient appears (for 3D plane crack problems) in Polch *et al.*[1987].